Journal of Translational Medicine

RESEARCH

Open Access

CircPRDM5-mediated regulation of miR-433-3p and HDAC6 in Parkinson's disease: a novel neuroprotective axis

Kai Wang[1,2*], Langfeng Zhu[3] and Zhibo Ren[3]

Abstract

Background Parkinson's disease (PD) is a progressive neurodegenerative disorder characterized by the loss of dopaminergic neurons, leading to motor and non-motor symptoms. Despite advances in PD research, the molecular mechanisms underlying its pathogenesis remain incompletely understood. Recent studies have highlighted the potential role of circular RNAs (circRNAs) in neurodegenerative diseases. This study aims to investigate the regulatory role of circPRDM5 in PD, focusing on its interactions with miR-433-3p and HDAC6.

Methods Bioinformatics tools were used to identify circPRDM5 and its potential interaction with miR-433-3p. Peripheral blood samples were collected from 20 PD patients and healthy controls to measure circPRDM5, miR-433-3p, and HDAC6 expression. For in vivo studies, an MPTP-induced PD mouse model was established, and circPRDM5 knockdown was achieved via tail vein injections of shRNA constructs. Behavioral tests, histological analysis, and immunohistochemistry were used to evaluate motor function and neuronal integrity. In vitro, SH-SY5Y neuroblastoma cells were treated with MPP^+ to induce PD-like characteristics, followed by transfection with circPRDM5 knockdown constructs and miR-433-3p mimics or inhibitors. Cell viability, lactate dehydrogenase (LDH) release, apoptosis, and autophagy were measured through CCK-8 assay, flow cytometry, western blotting, and immunofluorescence.

Results CircPRDM5 expression was significantly elevated in PD patients and MPTP-induced PD mice, with knockdown of circPRDM5 alleviating motor deficits and neuronal damage in vivo. In vitro, circPRDM5 knockdown in SH-SY5Y cells reduced MPP^+-induced cellular damage, apoptosis, and autophagy. Bioinformatics analysis identified miR-433-3p as a target of circPRDM5, and its downregulation in PD patients and MPP^+-treated cells was observed. Dual-luciferase and RNA pull-down assays confirmed that circPRDM5 functions as a sponge for miR-433-3p, which regulates HDAC6 expression. HDAC6 was found to be upregulated in PD and contributed to neuronal damage. Furthermore, HDAC6 overexpression reversed the protective effects of circPRDM5 knockdown, highlighting the role of the circPRDM5/miR-433-3p/HDAC6 axis in PD pathology.

Conclusions This study reveals that circPRDM5 promotes neuronal damage in PD by sponging miR-433-3p and upregulating HDAC6, contributing to apoptosis and autophagy. Knockdown of circPRDM5 reduces PD-like symptoms in both cellular and animal models, providing a potential therapeutic target for PD. Targeting the circPRDM5/miR-433-3p/HDAC6 axis may offer new opportunities for disease-modifying treatments in PD.

Keywords Parkinson's disease, CircPRDM5, MiR-433-3p, HDAC6, Autophagy, Apoptosis

*Correspondence:
Kai Wang
wangkai960708@163.com
Full list of author information is available at the end of the article

© The Author(s) 2025. **Open Access** This article is licensed under a Creative Commons Attribution-NonCommercial-NoDerivatives 4.0 International License, which permits any non-commercial use, sharing, distribution and reproduction in any medium or format, as long as you give appropriate credit to the original author(s) and the source, provide a link to the Creative Commons licence, and indicate if you modified the licensed material. You do not have permission under this licence to share adapted material derived from this article or parts of it. The images or other third party material in this article are included in the article's Creative Commons licence, unless indicated otherwise in a credit line to the material. If material is not included in the article's Creative Commons licence and your intended use is not permitted by statutory regulation or exceeds the permitted use, you will need to obtain permission directly from the copyright holder. To view a copy of this licence, visit http://creativecommons.org/licenses/by-nc-nd/4.0/.

Introduction

Parkinson's disease (PD) is a progressive neurodegenerative disorder, primarily characterized by the loss of dopaminergic neurons, which results in both motor and non-motor symptoms, such as bradykinesia, rigidity, and cognitive decline [1]. Despite significant advances in PD research, the precise molecular mechanisms underlying its pathogenesis remain incompletely understood [2]. Current therapeutic interventions primarily focus on symptom management, and no disease-modifying treatments are currently available [3, 4]. This gap underscores the critical need for further research aimed at identifying novel molecular targets that could pave the way for disease-modifying treatments.

Recent studies have highlighted the emerging role of circular RNAs (circRNAs), a class of non-coding RNAs, as key regulators in various biological processes, including neurodegeneration [5]. Unlike linear RNAs, circRNAs form covalently closed loop structures, making them highly resistant to exonuclease degradation and thus more stable [6]. These structural properties, coupled with their diverse biological functions-including acting as microRNA (miRNA) sponges, interacting with RNA-binding proteins, and potentially encoding peptides have brought circRNAs into focus in neurodegenerative diseases [7–9]. One such circRNA, circPRDM5 (hsa_circRNA_103730) has been studied extensively in the context of cancer, where it is implicated in regulating tumorigenesis through its interactions with various molecular pathways. For example, circPRDM5 suppresses gastric cancer cell proliferation, migration, invasion, and glucose metabolism by downregulating GCNT4 expression through the miR-485-3p pathway [10]. Similarly, the circ_PRDM5/miR-25-3p/ANKRD46 axis is linked to the promotion of malignant behaviors in breast cancer cells [11]. Besides cancer, circ-PRDM5 is also reported to promote human lens epithelial cell migration, invasion, and epithelial-to-mesenchymal transition (EMT) by sequestering miR-92b-3p and upregulating COL1 A2 expression [12]. CircPRDM5 has also been identified as a diagnostic biomarker for acute myocardial infarction [13]. In the context of neurodegenerative disorders, a recent study has reported elevated levels of circPRDM5 in PD patients [14], suggesting its possible role in PD pathogenesis. Yet its functional role and the underlying mechanism in neurodegenerative diseases such as PD remain unexplored. Thus, it raises intriguing questions about how circPRDM5 contributes to neurodegeneration and whether it interacts with other molecular pathways implicated in PD.

The interaction between circRNAs and miRNAs represents a key regulatory axis in many diseases. miRNAs, small non-coding RNAs, regulate gene expression at the post-transcriptional level by binding to the 3'untranslated region (3'UTR) of target mRNAs [15]. A growing body of evidence suggests that circRNAs can act as miRNA sponges, thereby modulating miRNA availability and influencing their downstream targets [16].

Among the various miRNAs, miR-433-3p, in particular, has been associated with neurodegenerative disorders. Research by Burgos et al. revealed that reduced miR-433 expression was present in cerebrospinal fluid in both Parkinson's disease and Alzheimer's disease patients [17]. Additionally, circulating miR-433 has been observed to be downregulated in PD patients compared to healthy individuals, making it a potential diagnostic biomarker [18]. Another study by Zhang et al. highlighted miR-433 regulatory impact on neuron proliferation and migration under hypoxic conditions [19], emphasizing its crucial role in regulating neural cell functions. Furthermore, miR-433 is reported to serve as a candidate diagnostic biomarker for AD patients [20]. However, the functional role and potential interactions between miR-433-3p and circPRDM5 in the context of PD have not been explored yet.

Histone deacetylase 6 (HDAC6), a member of the histone deacetylase family, is another molecule of interest in neurodegenerative diseases. HDAC6 has been shown to regulate autophagy, a key cellular process for degrading and recycling misfolded proteins, which is vital for maintaining neuronal health [21]. Autophagy dysfunction is a hallmark of many neurodegenerative diseases, and HDAC6 has been shown to specifically modulate autophagy in the context of neurodegeneration [22]. Its involvement in neurodegeneration has been highlighted in several studies, with HDAC6 activity being particularly relevant in the context of PD [23, 24]. However, its precise role as a downstream target of circRNA and miRNA interactions in PD has yet to be fully elucidated.

Given these findings, we hypothesized that circPRDM5 may exert neuroprotective effects by regulating the miR-433-3p/HDAC6 axis in the context of PD. The objective of this study was to investigate the mechanistic role of circPRDM5 in PD and to explore its potential interactions with miR-433-3p and HDAC6. Unraveling these molecular pathways could provide novel insights into the pathogenesis of PD and offer potential therapeutic targets for disease-modifying interventions.

Materials and methods

Bioinformatics analysis

The formation of circPRDM5, arising from the back-splicing of PRDM5 exons 8–14, was predicted using circPrimer (https://www.bio-inf.cn/), a widely used bioinformatics tool for identifying circular RNA splicing events. The binding sites for circPRDM5 and miR-433-3p

were identified using the CircInteractome platform (https://circinteractome.nia.nih.gov/). To explore the regulatory network, miRDB (http://www.mirdb.org/) was employed to analyze miR-433-3p interactions with its target genes, with a specific focus on HDAC6.

Patient sample collection

Ethical approval was granted by the appropriate institutional review boards (ethics approval number: 2020-624), and written informed consent was collected from all participants prior to the study. All procedures adhered to ethical and regulatory guidelines, ensuring compliance with the Declaration of Helsinki. Peripheral blood samples were obtained from patients with Parkinson's disease (PD) (n = 20) and age-matched healthy controls (n = 20) to assess biomarker expression levels. There were 9 male and 11 female healthy participants, with an average age of 67.2 ± 5.5. In the PD group, there were 10 males and 10 females with an average age of 67.6 ± 4.7. No statistically significant differences in age or sex distribution were observed between the two groups.

The severity of PD was assessed using the Hoehn-Yahr staging system, originally proposed in 1967 by Margaret Hoehn and Melvin Yahr, which categorizes disease progression into five stages (I–V) based on motor symptoms and functional impairment, with later stages indicating more severe disease [25]. In our cohort, the distribution of PD stages was as follows: stage I (n = 2), stage II (n = 4), stage III (n = 7), stage IV (n = 6), and stage V (n = 1). PD diagnosis was based on established clinical criteria, requiring the presence of bradykinesia along with at least one additional motor symptom: muscular rigidity (myotonia), resting tremor (4–6 Hz), or postural instability, with exclusions for primary visual, cerebellar, vestibular, or proprioceptive dysfunction [26].

The inclusion criteria for PD diagnosis included unilateral onset of symptoms, the presence of resting tremor, a positive response to levodopa therapy, development of severe anisocoria attributable to levodopa, gradual disease progression, sustained responsiveness to levodopa for over five years, asymmetrical motor involvement throughout the disease course, and a disease duration of more than ten years. Exclusion criteria encompassed a history of recurrent strokes leading to stepwise progression of parkinsonism, prior head trauma or brain injury, antipsychotic or dopamine-depleting drug use, confirmed history of encephalitis or non-drug-induced akinetic crises, prolonged remission of PD symptoms, lack of response to high-dose levodopa therapy (except in cases of malabsorption), and strictly unilateral symptom onset persisting for over three years. Further exclusions included the emergence of additional neurological signs such as supranuclear gaze palsy, cerebellar signs, early severe autonomic involvement, positive Babinski's sign, early-onset dementia, exposure to neurotoxins, neuroimaging evidence of intracranial tumors or hydrocephalus, and a history of autoimmune disease [4, 27–31].

Venous blood was drawn via standard venipuncture into serum separator tubes for serum collection and EDTA-coated tubes for plasma. Samples were processed within two hours of collection. Plasma and serum were separated by centrifugation at 1500 × g for 10 min at 4 °C. The resulting plasma and serum aliquots were stored at −80 °C for subsequent analyses.

Establishment of MPTP-induced PD mouse model

Eight-week-old male C57BL/6 mice, weighing approximately 25–30 g, were purchased from GemPharmaTech Co., Ltd. (Nanjing, China) and maintained under specific pathogen-free conditions at the animal facility. All animal procedures were approved by the Institutional Animal Care and Use Committee of our institution (ethics approval number: 2020-624). After one week of acclimatization, the mice were divided into two groups: MPTP group (n = 18) injected with MPTP (MPTP, CAS: 23007-85-4, Santa Cruz Biotechnology, USA) at a dose of 30 mg/kg intraperitoneally (i.p) once daily for 5 days, as used previously [32] and control group (n = 6) injected with an equal volume of saline (0.9% NaCl).

To investigate the in vivo effects of circPRDM5 knockdown, mice in the MPTP group were subdivided into three experimental groups (n = 6 per group): the MPTP group, the sh-NC group (negative control), and the sh-circPRDM5 group, with 6 mice in each group. Short hairpin RNA (shRNA) constructs targeting circPRDM5 and control (sh-NC) were designed and synthesized by Genscript (Shanghai, China) and cloned into viral vectors for systemic delivery. The shRNA vectors were administered via tail vein injection at a dose of 2 mg/kg to ensure efficient knockdown of circPRDM5. Following vector administration for 3 consecutive days, the animals were monitored for the development of PD-like symptoms. After completion of behavioral testing, mice were anesthetized using 10% chloral hydrate (3.5 mg/kg), and intracardiac perfusion was performed through the left ventricle using 0.9% saline. Whole brains were harvested, and relevant brain regions, including the substantia nigra (SN), were carefully dissected and preserved for subsequent analysis.

Behavioral tests

Pole test

The pole test was conducted using a wooden pole measuring 60 cm in height and 1 cm in diameter, with a 2-cm diameter wooden ball affixed at the top. To enhance grip and prevent slippage during the test, the pole was

wrapped with gauze. Mice were placed on the wooden ball at the top of the pole, and the time it took for each mouse to fully descend from the ball to the base of the pole was recorded as the latency to descend.

Rotarod test

The rotarod test was conducted using an automated apparatus with a 3-cm diameter rod to assess motor coordination and balance. Prior to testing, mice were acclimatized to the testing room and given a brief habituation session on a stationary rod. The test was performed in a controlled environment to minimize external variables. Mice were placed on the rod, which accelerated from 4 to 40 rpm over a 5-min period. The latency to fall (in seconds) was recorded, with a maximum score of 300 s if the mouse remained on the rod for the entire duration. Each mouse underwent three trials, with a 1-h inter-trial interval to minimize fatigue effects. The mean of the three trials was used for statistical analysis.

Open-field test

The open-field test was conducted in a square arena with dimensions of 40 ×40 ×40 cm, with the floor divided into 16 equal squares. The test was performed in a quiet room with consistent, moderate lighting, and mice were allowed to acclimatize to the environment for 30 min prior to testing. Mice were placed in the central square at the start of the test, and the number of squares crossed by each mouse over a 5-min period was recorded to assess locomotor activity and exploratory behavior. Between each test, the arena was thoroughly cleaned with 70% ethanol to prevent olfactory cues from influencing subsequent trials.

Hematoxylin and Eosin (HE) staining

The brain tissues were fixed in 4% paraformaldehyde solution overnight, dehydrated, cleared, and embedded in paraffin wax (PHC 6062, Poth Hille, USA). Tissue sections of 5 μm thickness were prepared using a microtome (Leica Biosystems). These sections were mounted on glass slides (KLINPR-001, VWR International, USA) for hematoxylin and eosin (H&E) staining. The staining procedure involved deparaffinization in xylene, followed by rehydration through a graded ethanol series (100%, 95%, 70%). The sections were then stained with hematoxylin (047223.22, Thermo Fisher, USA) to visualize nuclei, and counterstained with eosin (152885000, Thermo Fisher, USA) to highlight cytoplasmic components. After eosin staining, the slides were dehydrated in ascending concentrations of ethanol, cleared in xylene, and finally mounted with a coverslip. The stained sections were examined using a light microscope (DMI8, Leica) to assess morphological changes, cellular organization, and potential pathological changes.

Terminal deoxynucleotidyl transferase dutp nick end labeling (TUNEL) staining

Brain tissue samples were fixed in 4% paraformaldehyde at 4 °C for 24 h. The tissues were then cryoprotected in a sucrose solution, embedded in optimal cutting temperature (OCT) compound, and sectioned into 10 μm thick slices using a cryostat. Apoptosis was evaluated using a TUNEL assay kit (C10625, Thermo Fisher Scientific, USA) according to the manufacturer's instructions. Briefly, the sections were permeabilized with a detergent solution, incubated with 50 μL of TUNEL reaction mixture for one hour at 37 °C to label DNA strand breaks, and subsequently counterstained with DAPI for 10 min to visualize cell nuclei. TUNEL-positive cells, indicative of apoptosis, were quantified under a fluorescence microscope. The extent of neuronal apoptosis was evaluated by counting TUNEL-positive cells in the five visual fields from randomly chosen sections using ImageJ image analysis software and comparing them to control samples to assess neurodegeneration.

Immunohistochemistry (IHC) detection of tyrosine hydroxylase (TH) protein

Paraffin-embedded mouse brain tissue sections were processed for immunohistochemistry, including deparaffinization in xylene and rehydration through a graded ethanol series. Antigen retrieval was performed by heating the sections in a citrate buffer (pH 6.0). After cooling, the sections were blocked with 5% bovine serum albumin (BSA) for 1 h at room temperature to prevent nonspecific binding. The sections were then incubated overnight at 4 °C with a primary antibody against tyrosine hydroxylase (TH) (AB1521, EMD Millipore, USA) at a dilution of 1:500. The next day, an HRP-conjugated secondary antibody (7074, Cell Signaling, USA) was applied for 1 h at room temperature. Following the antibody incubation, the sections were developed using 3,3'-diaminobenzidine (DAB) as the chromogen, followed by hematoxylin counterstaining. Imaging of the stained sections was performed using a light microscope, and the optical density of TH-positive cells was quantified using ImageJ software.

Cell culture and construction of SH-SY5Y cell model of PD

Human neuroblastoma cells, SH-SY5Y, were purchased from Sigma-Aldrich company (94,030,304, Sigma-Aldrich, USA). The cells were cultured in Dulbecco's Modified Eagle Medium (DMEM)/F12 (SLM-243-B, Sigma-Aldrich, USA) supplemented with 10% fetal bovine serum (FBS) (CLARK, Virginia, U.S.) in an

incubator at 37 °C with 5% CO_2. To establish a cellular PD-like model in vitro, 1×10^5 SH-SY5Y cells/mL were seeded in a 96-well plate and then treated with different concentrations of 1-methyl-4-phenylpyridinium (MPP^+) for different time durations. Based on our initial results, we selected a dose of 1 mM of MPP^+ and a time duration of 48 h for subsequent assays.

Cell transfection

To achieve the downregulation of circPRDM5, short hairpin RNA (shRNA) specific to circPRDM5 (sh-circPRDM5) was synthesized by Genscript (Shanghai, China). Additionally, miR-433-3p mimics were generated to upregulate miR-433-3p expression, while inhibitors targeting miR-433-3p (anti-miR-433-3p) were generated to downregulate its activity. For HDAC6 overexpression studies, HDAC6 was cloned into the pcDNA3.1 vector (OE-HDAC6) which was designed and synthesized by GenePharma (Shanghai, China). When the cells reached 70–80% confluency, transfections were performed along with their respective negative controls using Lipofectamine 3000 reagent (L3000008, Thermo Fisher Scientific, Waltham, USA), according to the manufacturer's protocol.

Quantitative reverse transcription polymerase chain reaction (qRT-PCR)

Total RNA was extracted from cells or tissues using the RNeasy Mini Kit (74104, QIAGEN, USA) according to the manufacturer's protocol. Complementary DNA (cDNA) was synthesized using SuperScript IV Reverse Transcriptase (18090010, Thermo Fisher, USA). Quantitative PCR (qPCR) was performed using SYBR Green PCR Master Mix (4312704, Thermo Fisher, USA) in a QuantStudio 3 thermal cycler (Thermo Fisher, USA). Fluorescence signals were continuously monitored during thermal cycling to quantify gene amplification. Gene expression levels were normalized to either GAPDH or U6 expression as reference controls, and relative quantification was calculated using the $2^{-\Delta\Delta Ct}$ method. The following primers were used for the qRT-PCR reactions: circPRDM5: Forward Primer: TGGATGAGC ACAAGAGGAC, Reverse Primer: GCTGAAGTTAGC CATAATGCA; miR-433-3p: Forward Primer: GTGCAG GGTCCGAGGT, Reverse Primer: GTGCAGGGTCCG AGGT; HDAC6: Forward Primer: GGAGGTAAAGAA GAAAGGCA, Reverse Primer: GTTCAGATCCAT CCCTTGC; U6: Forward Primer: CTCGCTTCGGCA GCACA, Reverse Primer: AACGCTTCACGAATTTGC GT; GAPDH: Forward Primer: ACCAGGGAGGCTGCA GTCC, Reverse Primer: TCAGTTCGGAGCCCACAC GC.

RNase R treatment

Total RNA was extracted from SH-SY5Y cells using TRIzol reagent (Catalog #15596018, Invitrogen, USA), following the manufacturer's protocol. The extracted RNA samples were subsequently treated with 3 U/μg of RNase R (RNR07250, Epicentre, France) at 37 °C for 30 min. After treatment, the levels of circPRDM5 and linear PRDM5 RNA were quantified using qRT-PCR.

Actinomycin D (ActD) treatment

SH-SY5Y cells were treated with Actinomycin D (ActD) (5 μg/mL, A9415, Sigma-Aldrich, USA), a transcription inhibitor. Following ActD addition, cells were incubated for various time points (0, 6, 12, 18, and 24 h) to inhibit RNA synthesis over time. After each incubation period, the levels of circPRDM5 and linear PRDM5 were quantified using qRT-PCR.

Fluorescence in situ hybridization (FISH) assay

SH-SY5Y cells were fixed and permeabilized prior to the FISH assay. Probes specific to circPRDM5 were synthesized with a Cy3 fluorescent label. Hybridization was performed using the circPRDM5-specific FISH probe (FP-PRDM5-Cy3) at a concentration of 200 nM in hybridization buffer (H7033, Sigma-Aldrich, USA), followed by overnight incubation at 37 °C. After the hybridization step, the cells were counterstained with DAPI (D1306, Thermo Fisher, USA) at a concentration of 300 nM in PBS to visualize the nuclei. Fluorescent signals corresponding to circPRDM5 were visualized using a fluorescence microscope, allowing for the localization and quantification of circPRDM5 expression in SH-SY5Y cells.

Cell viability assay using cell counting kit-8 (CCK-8)

SH-SY5Y cells (1×10^4 cells per well) were treated with varying concentrations of MPP^+ (0, 0.5, 1, or 2 mM) and incubated for different time points (0, 12, 24, or 48 h). After the treatment, the Cell Counting Kit-8 (CCK-8) reagent (CK04-01, Dojindo Molecular Technologies, USA) was added to each well, and the cells were incubated for an additional 1 h at 37 °C in a humidified incubator. Following the incubation with CCK-8, absorbance was measured at 450 nm using a microplate reader to assess cell viability.

Detection of lactate dehydrogenase (LDH) release

Cellular cytotoxicity was assessed by measuring lactate dehydrogenase (LDH) release using the CyQUANT™ LDH Cytotoxicity Assay Kit (Thermo Fisher Scientific, USA). SH-SY5Y cells were seeded into 96-well plates at a density of 10,000 cells per well and treated with MPP^+

at various concentrations. After the designated incubation periods, supernatants from the cell cultures were collected, and LDH release was measured according to the manufacturer's protocol. The percentage of LDH release, indicating cytotoxicity, was calculated based on previously established methods [33].

Detection of apoptosis using flow cytometry

Flow cytometry was used to assess apoptosis rates in SH-SY5Y cells using the Annexin V-FITC/PI Apoptosis Detection Kit (BD Biosciences, USA) in accordance with the provided protocol. In brief, SH-SY5Y cells were collected after indicated treatments and washed twice with cold PBS to eliminate any remaining media. Afterwards, the cells were resuspended in 1X binding buffer at a density of 0.5×10^6 cells per mL. A total of 5 µL of Annexin V-FITC and 5 µL of propidium iodide (PI) were added to 100 µL of the cell solution, followed by incubation for 20 min at room temperature in the dark. Following staining, cells were acquired on the BD Accuri™ C6 flow cytometer (BD Biosciences, USA) and data was analyzed using the FlowJo software to evaluate the rate of apoptosis.

Western blot analysis

SH-SY5Y cell lysates from various experimental groups were prepared using RIPA lysis buffer (89900, Thermo Fisher, USA), and protein concentrations were determined using the Pierce™ BCA Protein Assay Kit (23225, Thermo Fisher, USA). Equal amounts of protein were subjected to SDS-PAGE and transferred onto polyvinylidene fluoride (PVDF) membranes (88518, Thermo Fisher, USA). After protein transfer, the membranes were blocked with 5% non-fat dry milk in TBST (Tris-buffered saline with 0.1% Tween-20) and then incubated with

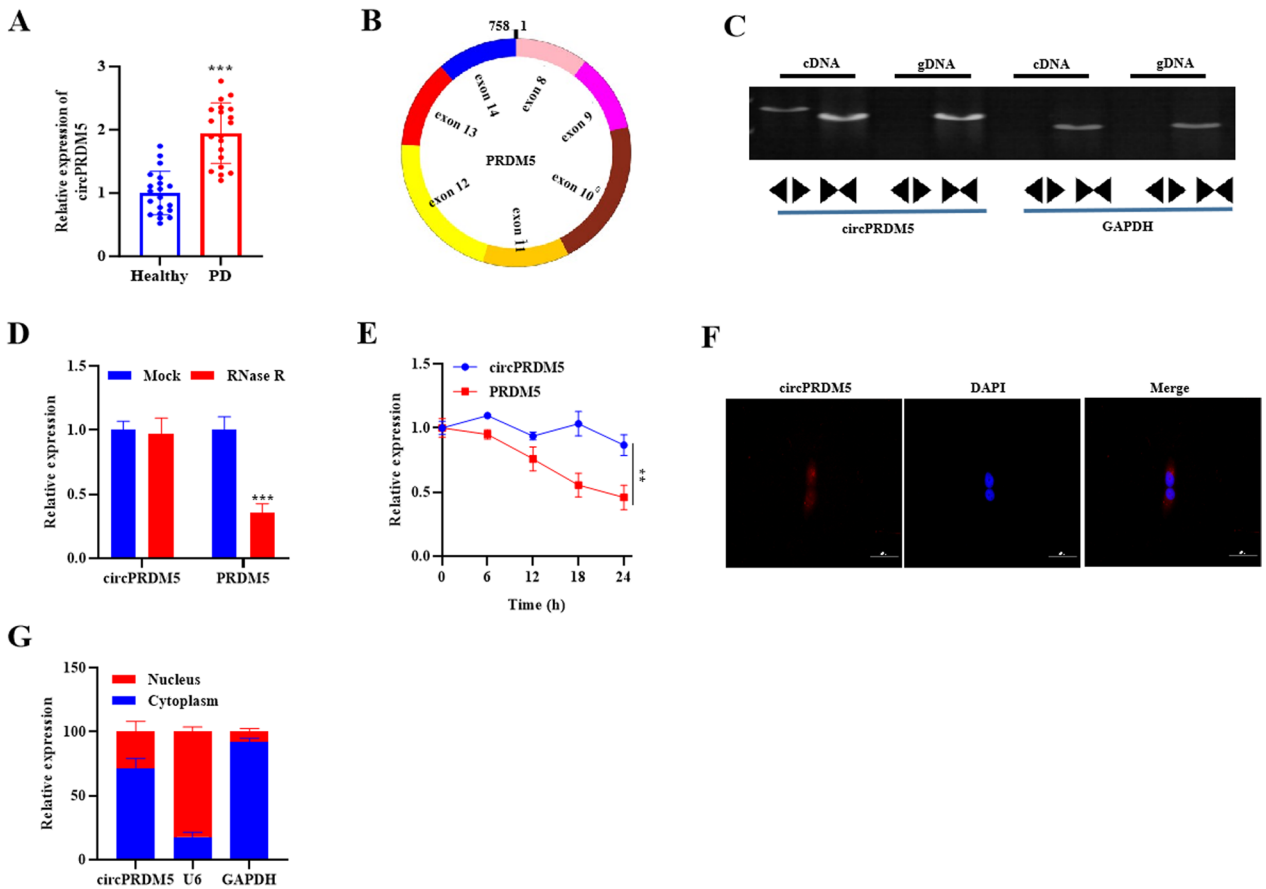

Fig. 1 Increased circPRDM5 expression in PD Patients. **A** qRT-PCR analysis of circPRDM5 expression in peripheral blood of healthy controls (n = 20) and PD Patients (n = 20). **B** circPrimer analysis of circPRDM5 splicing. **C** circPRDM5 amplification from cDNA or gDNA. **D** qRT-PCR analysis after RNase R treatment in SH-SY5Y cells. **E** qRT-PCR analysis after ActD treatment in SH-SY5Y Cells. **F** FISH assay was performed to evaluate circPRDM5 subcellular localization in SH-SY5Y cells (scale bar = 50 µm). **G** qRT-PCR analysis of circPRDM5 expression in cytoplasm and nucleus of SH-SY5Y cells. Data are shown as the mean ± SD of three different experiments, and statistical analyses were performed using unpaired Student's t-test. **p < 0.01, ***p < 0.001

the following primary antibodies overnight at 4 °C: Bax (5023S, 1:1000, Cell Signaling Technology, USA), Bcl-2 (2876S, 1:1000, Cell Signaling Technology, USA), LC3 I/II (12741S, 1:1000, Cell Signaling Technology, USA), p62/SQSTM1 (5114S, 1:1000, Cell Signaling Technology, USA), HDAC6 (7558S, 1:1000, Cell Signaling Technology, USA), and β-actin (3700, 1:1000, Cell Signaling Technology, USA) as a loading control. Following primary antibody incubation, the membranes were washed and incubated with horseradish peroxidase (HRP)-conjugated secondary antibody (SC-2005, 1:5000, Santa Cruz Biotechnology, USA) for 1 h at room temperature. Protein bands were detected using an enhanced chemiluminescence (ECL) substrate (32109, Thermo Fisher, USA), and their intensities were quantified using ImageJ software.

Immunofluorescence (IF) staining

Immunofluorescence staining was performed to visualize the subcellular localization of LC3 in treated SH-SY5Y cells. Following fixation and permeabilization, the cells were blocked with 5% bovine serum albumin (BSA) in PBS for 1 h at room temperature to reduce nonspecific binding. Cells were then incubated overnight at 4 °C with an anti-LC3 primary antibody (14600-1-AP, Cell Signaling Technology, USA). After washing with PBS, the cells were incubated with a FITC-conjugated secondary antibody (SA00003-2, Proteintech Group, USA) for 1 h at room temperature. Nuclear staining was performed using DAPI (62248, 1 mg/mL, Thermo Fisher, USA) for 5 min. Finally, coverslips were mounted onto slides with an antifade mounting medium, and images were captured using a Zeiss fluorescence microscope (Zeiss, Germany). The fluorescence intensity of LC3 staining was quantified using ImageJ software, allowing for the analysis of LC3 subcellular distribution in response to the treatments.

Dual-Luciferase reporter assay

The dual luciferase reporter assay was used to investigate the interaction between circPRDM5 and miR-433-3p, as well as miR-433-3p and HDAC6. Briefly, the 3'untranslated region (3'UTR) of circPRDM5 or HDAC6, containing the predicted miR-433-3p binding sites, was cloned downstream of the firefly luciferase gene in the pGL3 vector (E1751, Promega, USA). SH-SY5Y cells were then co-transfected with the pGL3 constructs and miR-433-3p mimics or negative control (NC) mimics using Lipofectamine 2000 (11668019, Invitrogen, USA). After 48 h of incubation, the luciferase activities were measured using the Dual-Luciferase Reporter Assay System (E1910, Promega, USA). Firefly luciferase activity was normalized to Renilla luciferase activity to account for transfection efficiency, and the relative luciferase activity was calculated to assess the interaction between the miRNA and its target sequences.

RNA pull-down assay

Biotin-labeled circPRDM5 probes and biotin-labeled control probes were synthesized (89818, Thermo Fisher, USA) for the RNA pull-down assay. SH-SY5Y cells were lysed using RIP lysis buffer (R0278, Sigma-Aldrich, USA), and the cell lysates were incubated with the biotin-labeled probes at 4 °C for 4 h to allow binding of target RNA molecules. Streptavidin-conjugated magnetic beads (88816, Thermo Fisher, USA) were then added to the mixture and incubated for an additional 2 h at 4 °C. Following several washes to remove unbound materials, the RNA complexes bound to the beads were eluted, and the extracted RNA was analyzed by qRT-PCR to detect the presence of miR-433-3p.

Statistical analysis

Statistical analyses were performed using SPSS software version 22.0 (IBM, USA) and data are presented as the mean ± Standard Deviation (SD) from at least three independent experiments. For comparisons between the two groups, an unpaired Student's t-test was conducted, ensuring that the assumptions of normality were met. For multiple group comparisons, one-way analysis of variance (ANOVA) followed by the Bonferroni post hoc test was used. A p-value of <0.05 was considered statistically significant for all tests.

Results

Expression characteristics of circPRDM5 in PD patients

We first aimed to investigate the expression levels of circPRDM5 (hsa_circRNA_103730) in Parkinson's disease (PD) patients. Through qRT-PCR analysis, we observed a significant increase in circPRDM5 levels in the peripheral blood of PD patients compared to healthy controls ($p<0.001$) (Fig. 1A). circPrimer analysis further confirmed that circPRDM5 is generated via reverse splicing of exons 8–14 of the PRDM5 gene (Fig. 1B). The circular nature of circPRDM5 was validated by amplification with divergent primers, demonstrating successful amplification of circPRDM5 in cDNA, but not in gDNA, confirming its circular nature (Fig. 1C). RNase R treatment further validated this, as circPRDM5 remained stable, while the linear form of PRDM5 was degraded ($p<0.001$) (Fig. 1D). Next, we evaluated the stability of circPRDM5 under transcriptional inhibition by Actinomycin D (ActD). Remarkably, circPRDM5 levels remained unchanged during the first 24 h of ActD treatment, further confirming its stability ($p<0.01$) (Fig. 1E).

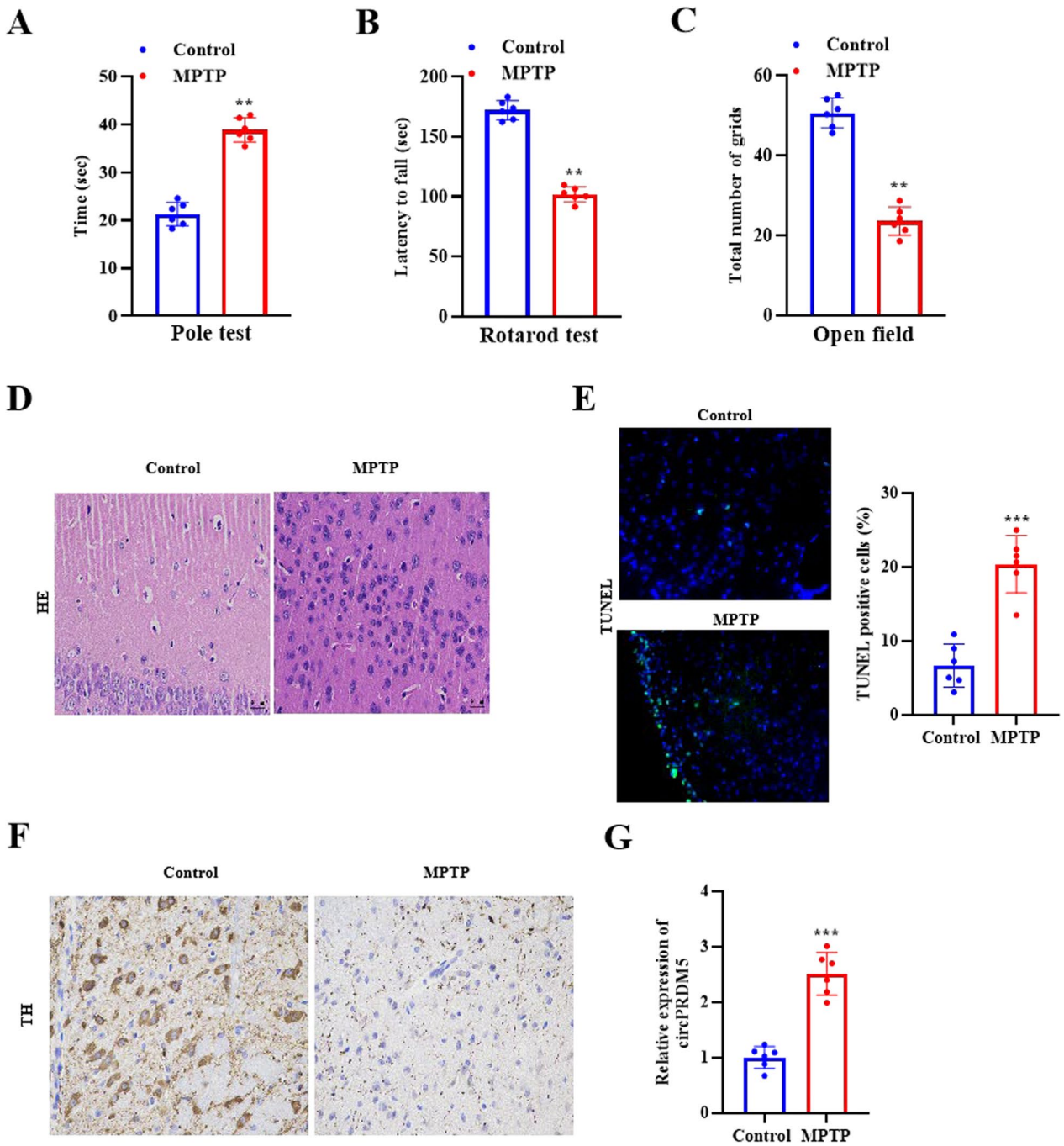

Fig. 2 Elevated expression of circPRDM5 contributes to PD-like pathological changes and motor dysfunction in MPTP-induced PD mouse model. **A**–**C** Pole test, rotarod test and open field test were implemented to evaluate motor function of mice in the control group (n = 6) and MPTP-induced PD group (n = 6). **D** HE staining of substantia nigra (SN) tissues from mice in the control group (n = 6) and MPTP group (n = 6) (scale bar = 20 μm). **E** TUNEL assay of SN tissues from mice in the control group (n = 6) and MPTP group (n = 6) (scale bar = 50 μm). **F** IHC staining of SN tissues from mice in the control group (n = 6) and MPTP group (n = 6) (scale bar = 20 μm). **G** qRT-PCR analysis of circPRDM5 levels in SN tissues from mice in the control group (n = 6) and MPTP group (n = 6). Data are shown as the mean ± SD from 6 mice per group, and statistical analyses were performed using unpaired Student's t-test. $^{**}p < 0.01$, $^{***}p < 0.001$

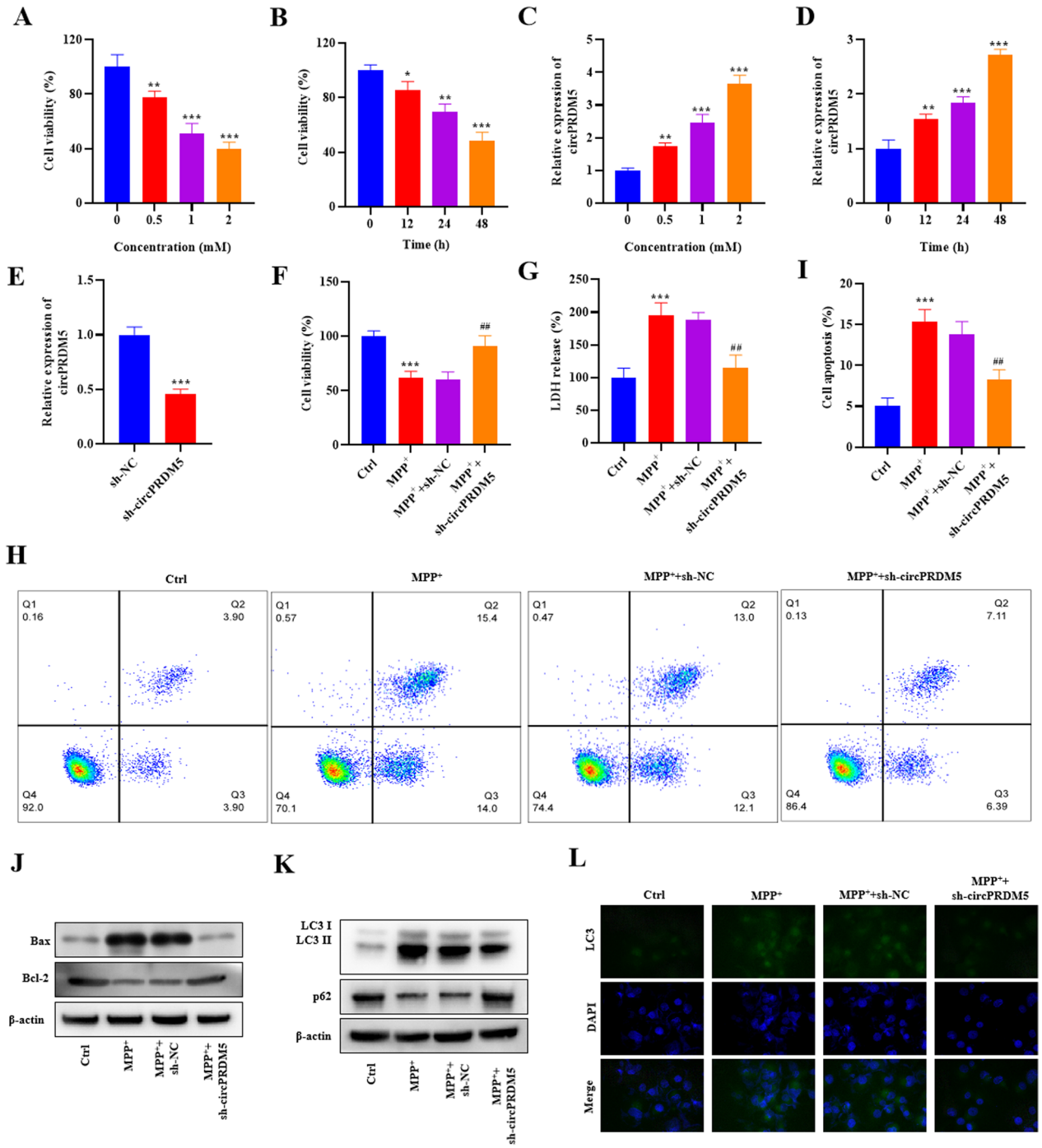

Fig. 3 Downregulation of circPRDM5 alleviates MPP^+-induced cellular damage, apoptosis, and autophagy. **A** CCK8 cell viability assay for SH-SY5Y cells treated with 0, 0.5, 1, or 2 mM MPP^+ for 24 h. **B** CCK8 cell viability assay for SH-SY5Y cells treated with 1 mM MPP^+ at 0 h, 12 h, 24 h, or 48 h. **C**, **D** qRT-PCR analysis of circPRDM5 expression in SH-SY5Y cells treated with 0, 0.5, 1, or 2 mM MPP^+ or in SH-SY5Y cells treated with 1 mM MPP^+ at 0 h, 12 h, 24 h, or 48 h. **E** qRT-PCR analysis of circPRDM5 knockdown efficiency in SH-SY5Y cells of the sh-NC group and sh- circPRDM5 group without any treatment. **F** CCK8 cell viability assay in SH-SY5Y cells left untreated or treated with 1 mM of MPP^+ for 48 h of the control group, MPP^+ group, MPP^+ + sh-NC group and MPP^+ + sh-circPRDM5 group. **G** LDH levels in SH-SY5Y cells of the indicated groups. **H**, **I** Flow cytometry analysis was performed to assess apoptosis rate in SH-SY5Y cells of the indicated groups. **J** Western blot assay for apoptosis-related proteins in SH-SY5Y cells of the indicated groups. **K** Western blot assay for autophagy-related proteins in SH-SY5Y cells of the indicated groups. **L** Immunofluorescence staining for LC3 protein in SH-SY5Y cells of the indicated groups (scale bar = 50 μm). Data are shown as the mean ± SD of three independent experiments. P values were calculated using either unpaired Student's t-test or one-way ANOVA followed by Bonferroni post hoc test. *$p < 0.05$, **$p < 0.01$, ***$p < 0.001$, $^{\#\#}p < 0.01$

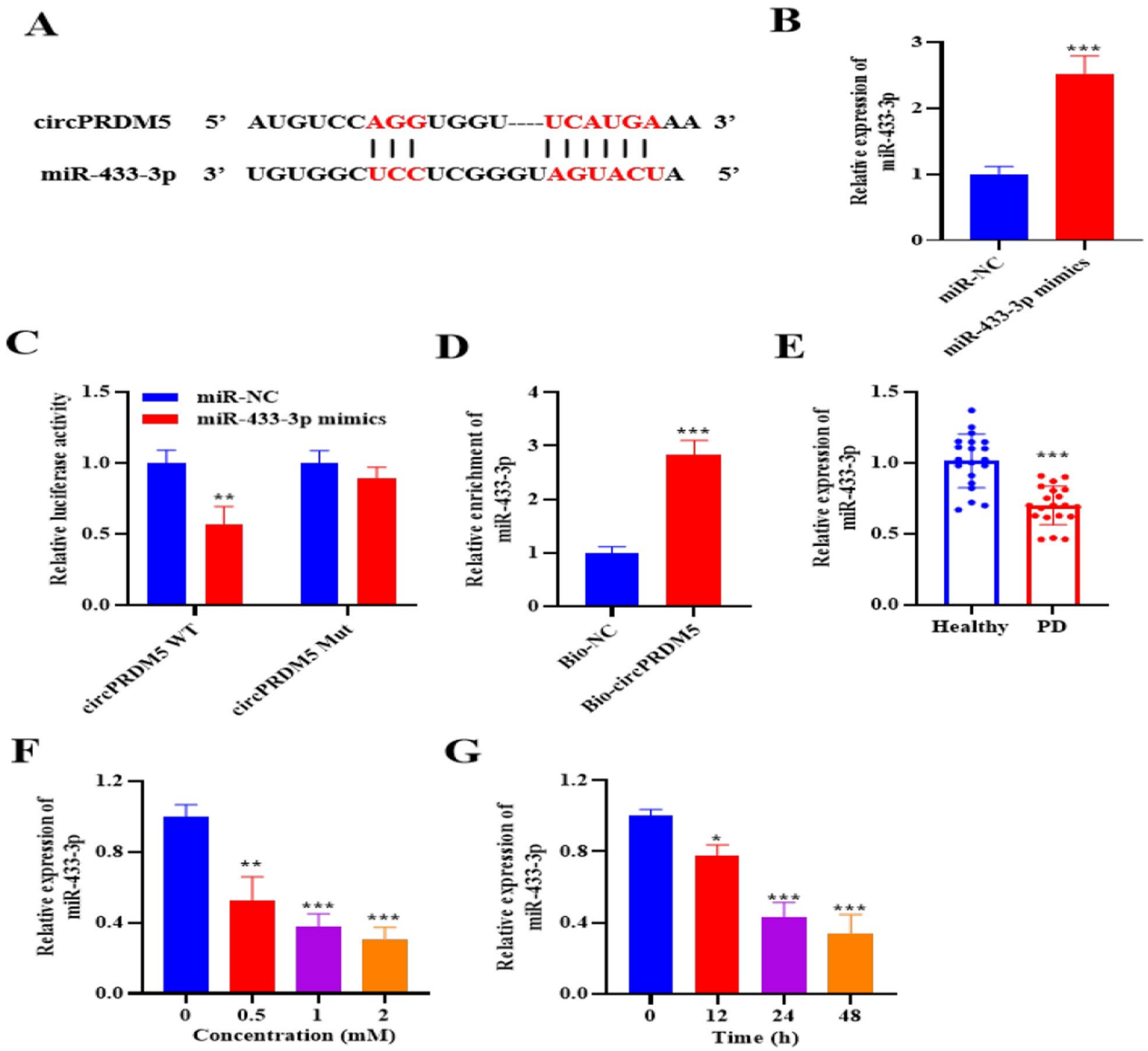

Fig. 4 CircPRDM5 sponges miR-433-3p. **A** Schematic representation of circPRDM5 binding site with miR-433-3p. **B** qRT-PCR analysis of miR-433-3p expression in SH-SY5Y cells transfected with miR-NC or miR-433-3p mimics. **C** Dual-luciferase reporter activity for WT/Mut group in SH-SY5Y cells transfected with miR-NC or miR-433-3p mimics. **D** RNA pull-down assay to assess the interaction between miR-433-3p and circPRDM5. **E** qRT-PCR analysis of miR-433-3p expression in peripheral blood samples of PD patients (n = 20) and healthy controls (n = 20). **F**–**G** qRT-PCR analysis of miR-433-3p expression in SH-SY5Y cells treated with different concentrations of MPP^+ for different time durations. Data are shown as the mean ± SD of three independent experiments. P values were calculated using either unpaired Student's t-test or one-way ANOVA followed by Bonferroni post hoc test. *p < 0.05, **p < 0.01, ***p < 0.001

Additionally, subcellular localization studies using FISH demonstrated that circPRDM5 predominantly resides in the cytoplasm (Fig. 1F, G). These results suggest that circPRDM5 expression is high in PD patients, exhibits stability and resistance to degradation, and is predominantly localized in the cytoplasm.

Elevated expression of circPRDM5 contributes to PD-like pathological changes and motor dysfunction in MPTP-induced PD mouse model

To further explore the relevance of circPRDM5 in PD, we established an MPTP-induced PD mouse model. Behavioral tests including the pole test, rotarod test, and open-field test were performed to evaluate the movement disorders, motor coordination, and spontaneous

locomotor activity of MPTP-induced PD mice. In comparison to control mice, MPTP-treated mice spent more time climbing down the pole and had shorter latencies in falling from the rotarod ($p < 0.01$) (Fig. 2A, B). Similarly, in the open-field test, MPTP-treated mice crossed fewer squares within 5 min compared to the control group mice ($p < 0.01$) (Fig. 2C). The results manifested that MPTP induction ameliorated the motor impairments of mice, suggesting the successful construction of the PD-like mouse model. Consistent with motor dysfunction, HE staining revealed significant neuronal shrinkage and morphological irregularities, with increased infiltration of inflammatory cells in brain tissues of the MPTP group compared to the control group mice (Fig. 2D). In addition, an increased number of TUNEL-positive neurons were found in the brain tissue of the MPTP-induced PD model group ($p < 0.001$) (Fig. 2E). Subsequently, IHC analysis also revealed a marked reduction in tyrosine hydroxylase (TH) protein levels, a marker of dopaminergic neurons, in the affected brain regions of the MPTP group compared to the control group mice (Fig. 2F). Notably, qRT-PCR revealed significantly increased circPRDM5 levels in MPTP-treated mice ($p < 0.001$) (Fig. 2G). These findings collectively suggest that circPRDM5 is upregulated in PD and may play a role in disease pathology.

Downregulation of circPRDM5 alleviates MPP^+-induced cellular damage, apoptosis, and autophagy

Given the increased expression of circPRDM5 in PD, we next sought to explore whether downregulating circPRDM5 could alleviate cellular damage induced by MPP^+, a neurotoxin commonly used to model PD-like characteristics in vitro. To this end, SH-SY5Y cells were treated with different concentrations of MPP^+ for various duration and cell viability was assessed using CCK-8 assays. The results revealed a dose- and time-dependent decrease in cell viability upon MPP^+ treatment ($p < 0.05$) (Fig. 3A, B). Correspondingly, qRT-PCR analysis confirmed that circPRDM5 expression increased with longer exposure to higher MPP^+ concentrations ($p < 0.001$) (Fig. 3C, D). Based on these results, we selected 1 mM MPP^+ for 48 h as the in vitro condition for subsequent experiments.

To explore the functional impact of circPRDM5, we knocked down its expression using shRNA (sh-circPRDM5). qRT-PCR confirmed successful knockdown of circPRDM5 ($p < 0.001$) (Fig. 3E). Interestingly, circPRDM5 knockdown significantly rescued the MPP^+-induced reduction in cell viability ($p < 0.01$) (Fig. 3F). Lactate dehydrogenase (LDH) release assays further indicated that downregulating circPRDM5 reduced LDH release induced by MPP^+, indicating a reduction in cellular damage ($p < 0.01$) (Fig. 3G). Flow cytometry revealed that enhanced apoptosis induced by MPP^+ was significantly reduced in circPRDM5-knockdown cells ($p < 0.01$) (Fig. 3H, I). Western blot analysis of apoptosis-related proteins Bax and Bcl-2 further supported the anti-apoptotic effect of circPRDM5 knockdown (Fig. 3J). Additionally, we investigated autophagy-related proteins using western blot and IF staining. The knockdown of circPRDM5 decreased MPP^+-induced autophagy, as evidenced by the altered expression of autophagy-related proteins and reduced LC3 staining (Fig. 3K, L). Collectively, these findings suggest that circPRDM5 downregulation attenuates MPP^+-induced cellular damage, apoptosis, and autophagy.

CircPRDM5 functions as a sponge against miR-433-3p

To investigate the molecular mechanism through which circPRDM5 exerts its effects, we utilized bioinformatics tool *CircInteractome* (https://circinteractome.nia.nih.gov/) to identify potential miRNA targets of circPRDM5. MiR-433-3p, previously reported as a biomarker in PD [18], was predicted to bind circPRDM5 (Fig. 4A). To validate this interaction, we transfected SH-SY5Y cells with miR-433-3p mimics, and qRT-PCR confirmed the efficiency of the transfection ($p < 0.001$) (Fig. 4B). Dual-luciferase reporter assays demonstrated significantly higher fluorescence intensity in cells transfected with wild-type circPRDM5 (circPRDM5 WT) compared to mutant circPRDM5 (circPRDM5 Mut) and miR-NC, indicating specific binding between circPRDM5 and miR-433-3p

(See figure on next page.)

Fig. 5 Neuroprotective effect of circPRDM5 knockdown is mediated by miR-433-3p. SH-SY5Y cells were first transfected with either short hairpin RNA (shRNA) specific to circPRDM5 (sh-circPRDM5) alone or together with miR-433-3p inhibitor (anti-miR-433-3p) or their corresponding negative control vectors. After transfection, the cells were either left untreated or treated with 1 mM of MPP^+ for 48 h. **A** qRT-PCR assay was performed to evaluate miR-433-3p expression in SH-SY5Y cells in indicated groups without any treatment. **B** CCK8 cell viability assay in SH-SY5Y cells of the sh-NC group, sh-circPRDM5 group, sh-circPRDM5 + anti-NC group and sh-circPRDM5 + anti-miR-433-3p group. **C** LDH levels in SH-SY5Y cells of the indicated groups. **D**, **E** Flow cytometry analysis was performed to assess apoptosis rate in SH-SY5Y cells of the indicated groups. **F** Western blot assay for apoptosis-related proteins in SH-SY5Y cells of the indicated groups. **G** Western blot assay for autophagy-related proteins in SH-SY5Y cells of the indicated groups. **H** Immunofluorescence staining for LC3 protein in SH-SY5Y cells of the indicated groups (scale bar = 50 μm). Data are shown as the mean ± SD of three independent experiments. P values were calculated using either unpaired Student's t-test or one-way ANOVA followed by Bonferroni post hoc test. $^{**}p < 0.01$, $^{***}p < 0.001$, $^{\#}p < 0.05$, $^{\#\#}p < 0.01$

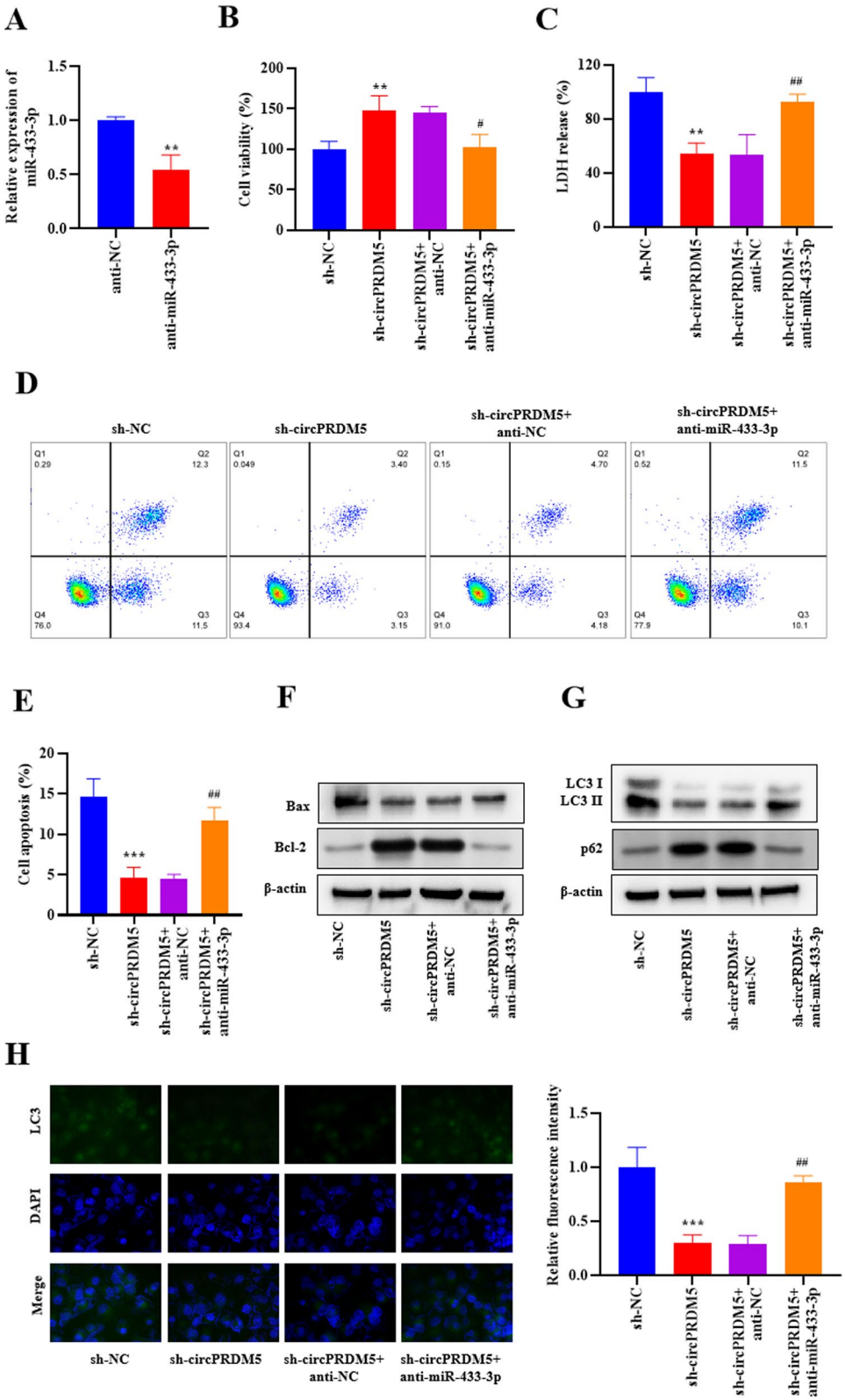

Fig. 5 (See legend on previous page.)

($p < 0.01$) (Fig. 4C). RNA pull-down assays further validated this interaction, showing significantly enhanced binding of Bio-circPRDM5 to miR-433-3p compared to the negative control (Bio-NC) ($p < 0.001$) (Fig. 4D). We then evaluated the expression level of miR-433-3p in healthy and PD patients. Analysis of peripheral blood from PD patients revealed a significant downregulation of miR-433-3p compared to healthy controls ($p < 0.001$) (Fig. 4E). Furthermore, we also noticed that MPP^+ treatment resulted in a dose- and time-dependent reduction in miR-433-3p expression ($p < 0.01$) (Fig. 4F, G). These results suggest that circPRDM5 may act as a sponge for miR-433-3p, potentially influencing miR-433-3p regulatory functions in PD pathology.

Neuroprotective effect of circPRDM5 knockdown is mediated by miR-433-3p

To further investigate the relationship between circPRDM5 and miR-433-3p, we assessed whether miR-433-3p mediates the neuroprotective effects of circPRDM5 knockdown. For this purpose, the anti-miR-433-3p vector was transfected into SH-SY5Y cells to inhibit miR-433-3p expression. qRT-PCR confirmed the successful knockdown of miR-433-3p (anti-miR-433-3p) ($p < 0.01$) (Fig. 5A). CCK-8 assay showed that the protective effects of circPRDM5 knockdown on cell viability were partially reversed by anti-miR-433-3p ($p < 0.05$) (Fig. 5B). Similarly, LDH assay demonstrated that the reduction in LDH release, indicative of reduced cell damage, observed with circPRDM5 knockdown was partially abrogated by anti-miR-433-3p ($p < 0.01$) (Fig. 5C). Flow cytometry revealed that the decrease in apoptosis induced by circPRDM5 knockdown was mitigated by anti-miR-433-3p ($p < 0.01$) (Fig. 5D, E). Western blot analysis also confirmed that apoptosis-related protein levels were similarly affected by anti-miR-433-3p, counteracting the effects of circPRDM5 knockdown (Fig. 5F). Western blot analysis and immunofluorescence staining of autophagy-related proteins revealed that miR-433-3p inhibition reversed the reduced autophagy observed in circPRDM5-knockdown cells ($p < 0.001$) (Fig. 5G, H). These findings suggest that circPRDM5 exerts its neuroprotective function through miR-433-3p.

miR-433-3p targets HDAC6

Given that miR-433-3p regulates neuroprotection, we sought to identify its downstream targets. Bioinformatics analysis revealed binding sites for miR-433-3p on the 3'UTR of HDAC6, a key regulator of neurodegenerative diseases (Fig. 6A). Both qRT-PCR and western blot analysis revealed a significant reduction in HDAC6 expression in SH-SY5Y cells transfected with miR-433-3p mimics compared to miR-NC, confirming miR-433-3p ability to suppress HDAC6 expression ($p < 0.01$) (Fig. 6B). Dual-luciferase reporter assays validated the direct interaction between miR-433-3p and HDAC6, as evidenced by decreased fluorescence intensity in HDAC6 WT constructs in the presence of miR-433-3p compared to miR-NC, further validating the direct interaction ($p < 0.001$) (Fig. 6C). RNA pull-down assays also demonstrated significant enrichment of miR-433-3p in the Bio-circPRDM5 group compared to the control ($p < 0.001$) (Fig. 6D). Interestingly, examination of peripheral blood samples revealed elevated HDAC6 levels in PD patients compared to healthy controls ($p < 0.001$) (Fig. 6E). Similarly, MPP^+ treatment led to a dose- and time-dependent increase in HDAC6 expression, as evident by both qRT-PCR and western blot analysis ($p < 0.01$) (Fig. 6F, G). Importantly, circPRDM5 knockdown significantly reduced HDAC6 expression in the MPP^+ model, which was partially reversed by miR-433-3p inhibition ($p < 0.01$) (Fig. 6H). These results suggest that HDAC6 is a direct target of miR-433-3p, and its expression is regulated by the circPRDM5/miR-433-3p axis.

CircPRDM5 promotes MPP.$^+$-induced neuronal damage via HDAC6

To determine the role of HDAC6 in circPRDM5-mediated neuronal damage, we overexpressed HDAC6 in SH-SY5Y cells. Overexpression of HDAC6 was confirmed via qRT-PCR ($p < 0.01$) (Fig. 7A). CCK-8 assay revealed that HDAC6 overexpression reversed the increased cell viability observed in the sh-circPRDM5 group ($p < 0.05$)

(See figure on next page.)

Fig. 6 HDAC6 is a direct target of miR-433-3p. **A** miRDB analysis of miR-433-3p binding sites in HDAC6. **B** qRT-PCR and western blot analysis of HDAC6 expression in SH-SY5Y cells transfected with either miR-NC or miR-433-3p mimics. **C** Dual-luciferase reporter activity for WT/Mut groups in SH-SY5Y cells transfected with either miR-NC or miR-433-3p mimics. **D** RNA pull-down assay was performed to assess the binding ability between miR-433-3p and HDAC6. **E** qRT-PCR analysis of HDAC6 expression in the peripheral blood samples of PD patients (n = 20) and healthy control (n = 20). **F**, **G** qRT-PCR and western blot analysis of HDAC6 expression in SH-SY5Y cells either treated with different concentrations of MPP^+ (0, 0.5, 1 or 2 mM) or with 1 mM of MPP^+ for different time duration (0, 12, 24 or 48 h). **H** qRT-PCR analysis of HDAC6 expression in SH-SY5Y cells left untreated or treated with 1 mM of MPP^+ for 48 h of sh-NC group, sh-circPRDM5 group, sh-circPRDM5 + anti-NC group, and sh-circPRDM5 + anti-miR-433-3p group. Data are shown as the mean ± SD of three independent experiments. P values were calculated using either unpaired Student's t-test or one-way ANOVA followed by Bonferroni post hoc test. $^{**}p < 0.01$, $^{***}p < 0.001$, $^{\#\#}p < 0.01$

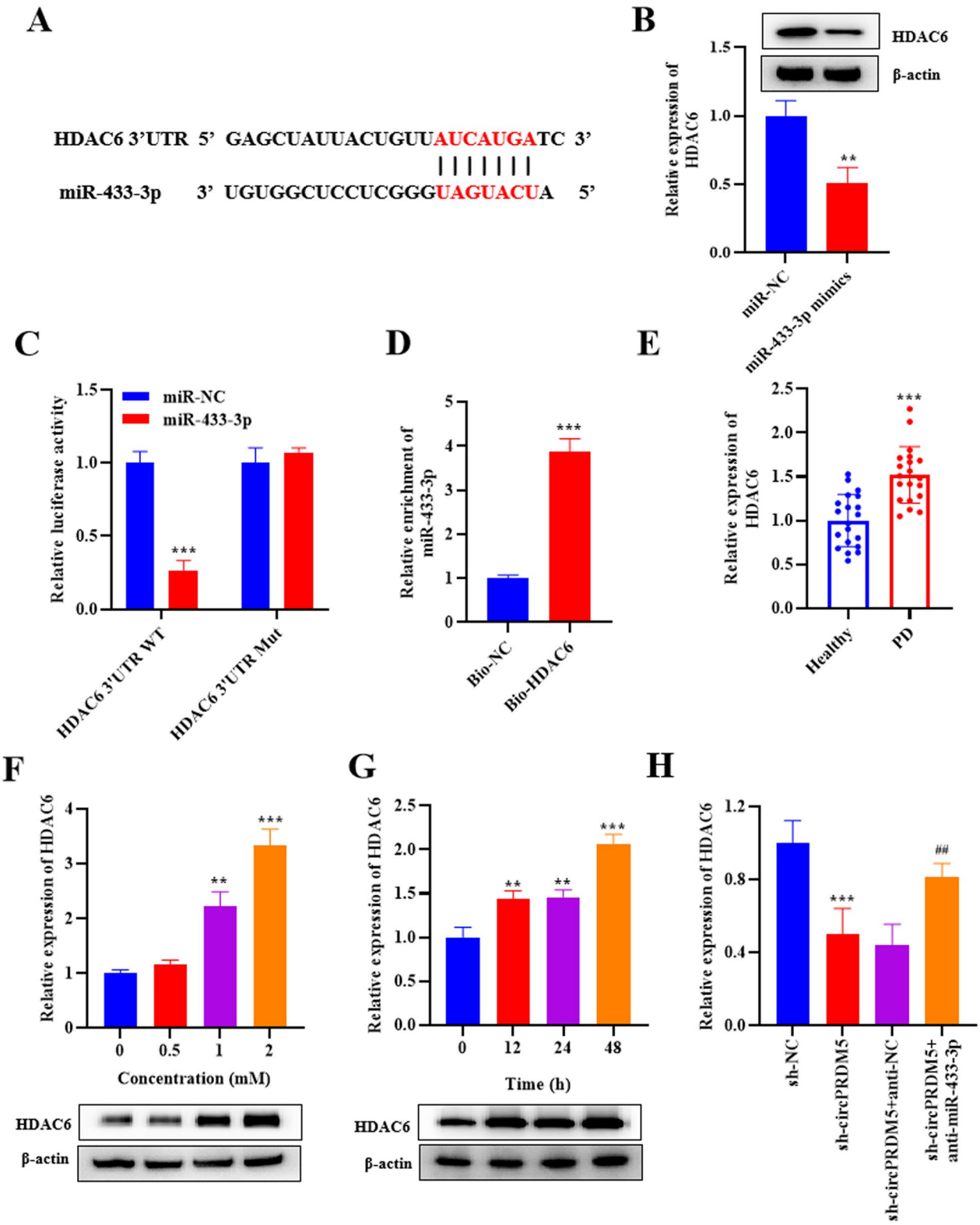

Fig. 6 (See legend on previous page.)

(Fig. 7B). LDH assay similarly demonstrated that HDAC6 overexpression restored the increased LDH release in the sh-circPRDM5 group ($p < 0.01$) (Fig. 7C). Furthermore, flow cytometry analysis showed that HDAC6 overexpression reversed the reduction in apoptosis observed in circPRDM5-knockdown cells ($p < 0.001$) (Fig. 7D). Western blot analysis further confirmed that HDAC6 overexpression reversed the alterations in apoptosis-related proteins (Bax and Bcl-2) induced by circPRDM5 knockdown (Fig. 7E). Additionally, HDAC6 overexpression reversed the effects of circPRDM5 knockdown on autophagy-related proteins LC3 I/II and p62 ($p < 0.01$) (Fig. 7F, G). These results suggest that circPRDM5 promotes neuronal damage in PD by upregulating HDAC6, and its downregulation can mitigate these effects.

CircPRDM5 knockdown alleviates PD symptoms in MPTP-induced mice

Lastly, we evaluated the therapeutic potential of circPRDM5 knockdown in an MPTP-induced PD mouse model. Data showed that the mice injected with sh-circPRDM5 had a shorter time to climb off the pole, a longer latency period to fall off the rotating pole, and more squares to pass through within 5 min compared to the mice injected with sh-NC ($p < 0.05$) (Fig. 8A–C). As expected, mice injected with sh-circPRDM5 exhibited reduced levels of circPRDM5 in brain tissue compared to the mice injected with sh-NC ($p < 0.001$) (Fig. 8D). HE staining of brain tissue revealed that circPRDM5 knockdown improved neuronal organization and reduced cellular disorganization compared to controls (Fig. 8E). Similarly, TUNEL staining showed a reduction in apoptotic cells in the MPTP + sh-circPRDM5 group ($p < 0.05$) (Fig. 8F), and IHC analysis demonstrated increased TH protein levels, suggesting a protective effect of circPRDM5 knockdown on dopaminergic neurons (Fig. 8G). Additionally, HDAC6 protein levels were significantly reduced in the sh-circPRDM5 group (Fig. 8H). These findings collectively suggest that circPRDM5 knockdown alleviates PD symptoms in mice by reducing HDAC6 expression and improving neuronal survival.

Discussion

PD is a devastating neurodegenerative condition characterized by the gradual degeneration of dopaminergic neurons within the substantia nigra region of the brain, resulting in a spectrum of motor and non-motor symptoms. This research delves into the intricate involvement of circPRDM5, miR-433-3p, and HDAC6 in the context of PD, elucidating the underlying molecular mechanisms and offering valuable insights into potential therapeutic avenues.

Our findings contribute to the expanding evidence that implicates circular RNAs (circRNAs) in PD pathogenesis [34]. Specifically, our study demonstrates that circPRDM5 levels are elevated in the blood of PD patients and that circPRDM5 exerts a protective effect against MPP^+-induced neuronal damage and MPTP-induced motor deficits. Tyrosine hydroxylase (TH), the rate-limiting enzyme in dopamine synthesis, declines to critical levels in PD, resulting in the onset of motor symptoms [35]. We observed that circPRDM5 knockdown exacerbates MPTP-induced TH reduction and promotes neuronal apoptosis. This protective function parallels findings with other circRNAs, such as circEPS15, which mitigates neuronal injury through the enhancement of PINK1-PRKN-mediated mitophagy [36]. Likewise, circPank1 has been shown to regulate the miR-7a-5p/α-synuclein axis, promoting neurodegeneration in dopaminergic neurons [37]. Further investigations have linked circSLC8 A1 to oxidative stress, with its expression elevated in cells exposed to oxidative stress and reduced upon treatment with the antioxidant simvastatin [38]. Consistent with these findings, we demonstrated that circPRDM5 knockdown alleviates MPP^+-induced neuronal damage. This was further supported by observations of reduced PD symptoms in a mouse model following circPRDM5 knockdown. This is consistent with the study of circSV2b [39], which also exacerbates PD pathology.

Autophagy, the cellular process of degrading and recycling proteins and organelles, is closely linked to PD pathogenesis [40]. Several studies have shown

(See figure on next page.)

Fig. 7 CircPRDM5 promotes MPP^+-induced neuronal damage via HDAC6. SH-SY5Y cells were first transfected with either sh-circPRDM5 alone or together with the HDAC6 overexpression vector (OE-HDAC6) or their corresponding negative control vectors. After transfection, the cells were left untreated or treated with 1 mM MPP^+ for 48 h. **A** qRT-PCR analysis was performed to assess HDAC6 expression in indicated groups of SY5Y cells without any treatment. **B** CCK8 cell viability assay in SH-SY5Y cells of the sh-NC group, sh-circPRDM5 group, sh-circPRDM5 + OE-NC group and sh-circPRDM5 + OE-HDAC6 group. **C** LDH levels in SH-SY5Y cells of the indicated groups. **D** Flow cytometry analysis was performed to assess apoptosis rate in SH-SY5Y cells of the indicated groups. **E** Western blot assay for apoptosis-related proteins in SH-SY5Y cells of the indicated groups. **F** Western blot assay for autophagy-related proteins in SH-SY5Y cells of the indicated groups. **G** Immunofluorescence staining for LC3 protein in SH-SY5Y cells of the indicated groups (scale bar = 50 μm). Data are shown as the mean ± SD of three independent experiments. P values were calculated using either unpaired Student's t-test or one-way ANOVA followed by Bonferroni post hoc test. $^{**}p < 0.01$, $^{***}p < 0.001$, $^{\#}p < 0.05$, $^{\#\#}p < 0.01$, $^{\#\#\#}p < 0.001$

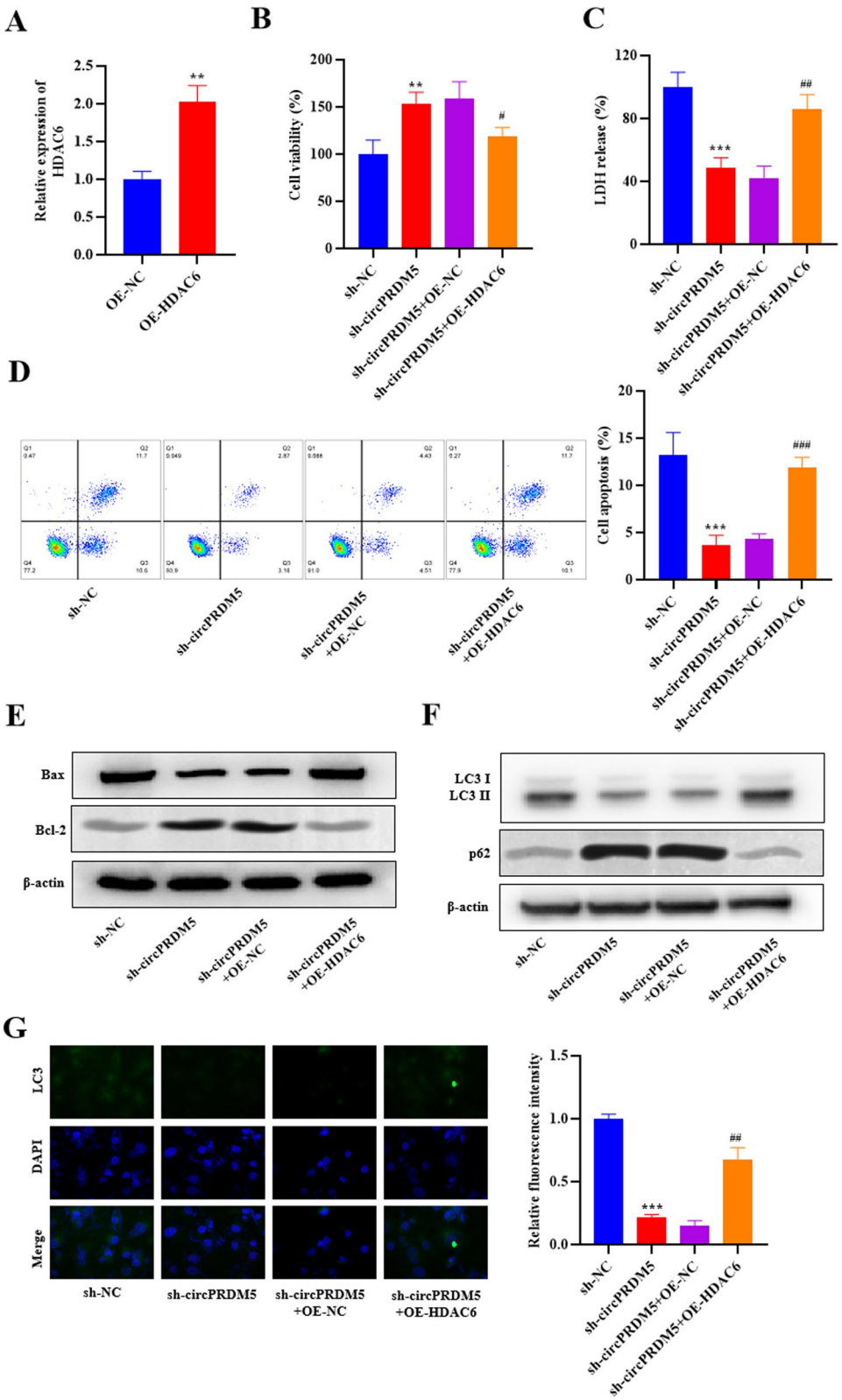

Fig. 7 (See legend on previous page.)

an accumulation of autophagosomes in the brains of PD patients and in MPTP-induced PD animal models [41–43]. Autophagy is characterized by increased LC3B-II/LC3B-I ratio and decreased SQSTM1/p62 levels. Neuronal autophagy is mainly a protective process in the nervous system; however, excessive autophagy is also associated with neuronal loss [44]. It has been reported that autophagosomes significantly accumulate in the brain tissues of PD patients and in MPTP-induced PD animal models [45, 46]. Previously, it has been shown that the long non-coding RNA NEAT1 promotes autophagy and apoptosis in MPTP-induced PD by impairing miR-374c-5p [47]. Another study reported that 7,8-dihydroxyflavone ameliorates motor deficits by regulating autophagy in MPTP-induced PD mice [48]. Similarly, melatonin is reported to attenuate MPTP-induced neurotoxicity by preventing CDK5-mediated autophagy and SNCA/α-synuclein aggregation [49]. In line with these reports, we also found in our study that circPRDM5 knockdown inhibits MPP^+-induced autophagy and apoptosis in SH-SY5Y cells. These results suggest that circPRDM5 knockdown mitigates MPP^+-induced apoptosis and autophagy, thereby reducing neuronal damage.

Moreover, our research identified a significant interaction between circPRDM5 and miR-433-3p. MPP^+ exposure led to decreased miR-433-3p levels, and circPRDM5 knockdown reduced cell viability and increased apoptosis in SH-SY5Y cells treated with MPP^+. Interestingly, these effects were reversed by anti-miR-433-3p treatment, demonstrating circPRDM5 neuroprotective role via modulation of miR-433-3p. These findings corroborate the growing body of evidence highlighting the significance of miRNAs and circRNAs in PD. For instance, in 2017, circulating levels of miR-433 were found to be significantly reduced in PD patients [18]. Furthermore, a study identified a connection between variations in the miRNA-433 binding site of FGF20 and an increased risk of PD, potentially through the overexpression of α-Synuclein [50]. Additionally, previous studies have highlighted the potential of circulating miRNAs as diagnostic biomarkers for PD, reinforcing our findings [51, 52].

We further demonstrated that miR-433-3p targets HDAC6, leading to a decrease in its expression. Moreover, HDAC6 expression is elevated in peripheral blood samples of PD patients, further highlighting its relevance to the disease. Zhao et al. suggest that HDAC6 depletion results in moderate alterations of behaviors and PD pathology in mice [53]. Another study demonstrated that HDAC6 suppression attenuates inflammatory response and protects dopaminergic neurons in PD [23]. We further delved into the intricate interplay between circPRDM5 and HDAC6 in the context of neuroprotection. The results showed that HDAC6 overexpression successfully reversed the adverse effects induced by circPRDM5 knockdown, as evidenced by increased cell viability, reduced apoptosis, and alterations in apoptosis- and autophagy-related proteins. Su et al. have suggested that HDAC6 regulates the aggresome-autophagy degradation pathway of α-synuclein in response to MPP^+-induced stress [54]. These results align with the growing body of research highlighting the critical roles of miRNAs and HDACs in PD. For example, miR-433-3p has been shown to inhibit bone formation and key osteoblast-related mRNAs [55]. Furthermore, studies have demonstrated that miR-433 can decrease endogenous HDAC6 expression [56], and influence the expression of an enhanced green fluorescent protein harboring the wild-type 3'-UTR of HDAC6 [57]. Additionally, recent reviews emphasize the unique role of HDAC6 among HDAC family members in neurodegeneration [58], with emerging evidence suggesting that HDAC6 inhibition could enhance cellular structural integrity and provide neuroprotection [59].

Despite our promising results, there are several limitations to this study. While our findings suggest therapeutic potential in targeting circPRDM5, miR-433-3p, and HDAC6 for PD, further research is needed to validate these conclusions in clinical settings. The sample size of this study is relatively small, which might limit the generalization of the results. Also, we did not explore the involved signaling pathways through which the circPRDM5/miR-433-3p/HDAC6 axis mediates its function, which needs further investigation. Moreover, our study predominantly used in vitro and animal models and translating these results to human patients may present challenges. Future studies should focus on preclinical and

(See figure on next page.)

Fig. 8 CircPRDM5 knockdown alleviates PD symptoms in MPTP-induced mice. **A**–**C** Pole test, rotarod test and open field test were implemented to evaluate the motor function of mice in the MPTP + sh-NC group (n = 6) and MPTP + sh-circPRDM5 group (n = 6). **D** qRT-PCR analysis of circPRDM5 expression in substantia nigra (SN) tissue samples from mice in MPTP + sh-NC group (n = 6) and MPTP + sh-circPRDM5 group (n = 6). **E** HE staining of SN samples from indicated groups of mice (n = 6) (scale bar = 20 μm). **F** TUNEL staining of SN samples from indicated groups of mice (n = 6) (scale bar = 50 μm). **G** Immunohistochemical detection of TH and HDAC6 expression in SN samples from mice in the indicated groups (n = 6) (scale bar = 20 μm). **H** Western blot detection of HDAC6 protein in SN samples from indicated groups of mice (n = 6). Data are shown as the mean ± SD from 6 mice per group, and statistical analyses were performed using unpaired Student's t-test. *p < 0.05, **p < 0.01, ***p < 0.001

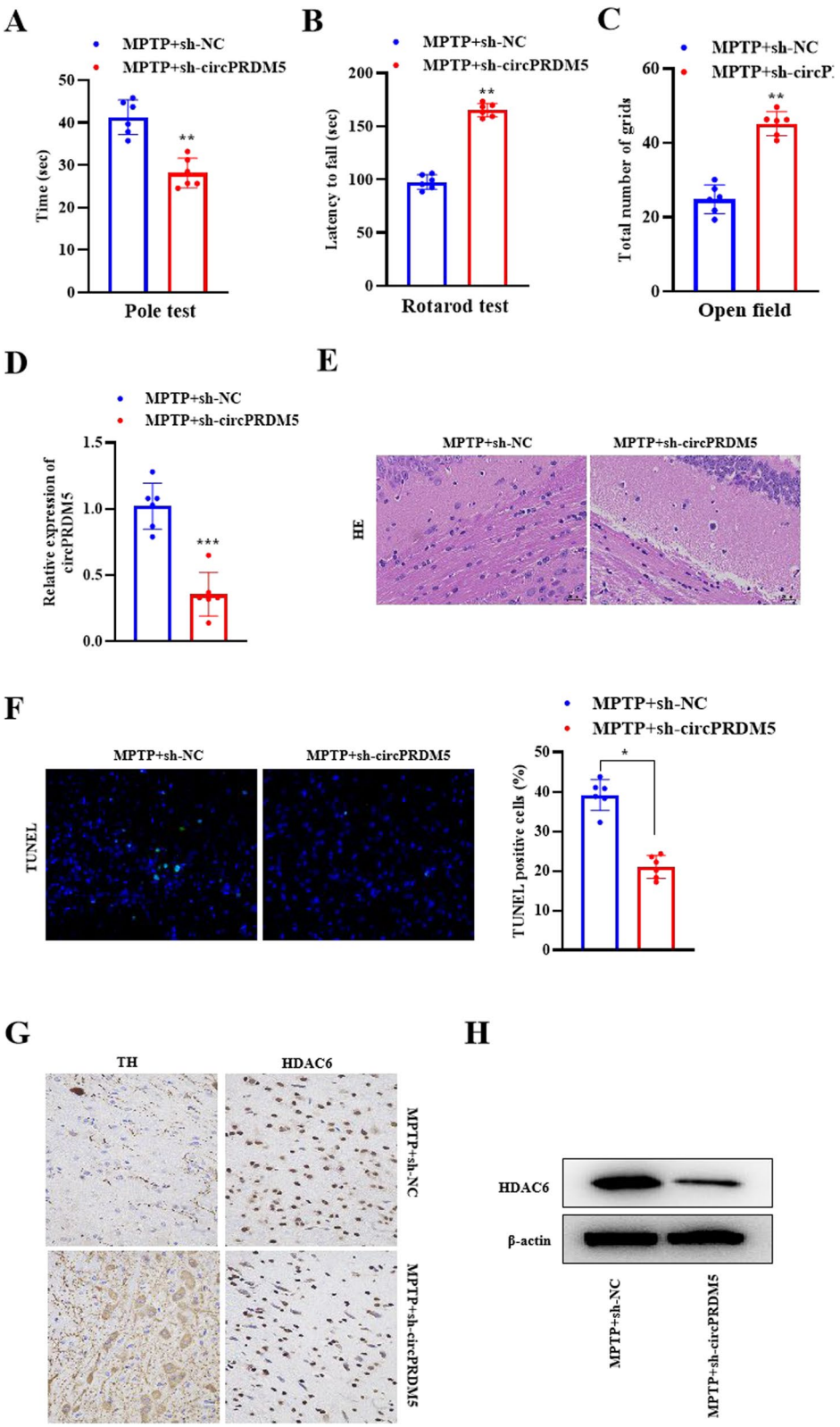

Fig. 8 (See legend on previous page.)

clinical trials to assess the safety and efficacy of potential interventions.

Conclusions

This study highlights the critical role of the circPRDM5/miR-433-3p/HDAC6 axis in PD pathogenesis. We demonstrated that circPRDM5 is upregulated in PD and promotes neuronal damage by regulating miR-433-3p and HDAC6, which control apoptosis and autophagy processes. Importantly, the knockdown of circPRDM5 alleviates PD-like symptoms in vitro and in vivo, highlighting its potential as a therapeutic target. These findings suggest that targeting the circPRDM5/miR-433-3p/HDAC6 axis could offer new therapeutic avenues for PD.

List of abbreviations

ActD	Actinomycin D
AD	Alzheimer's disease
ANOVA	Analysis of variance
RIP	Radioimmunoprecipitation
Bax	BCL2-associated X protein
Bcl-2	B-cell lymphoma-2
BSA	Bovine serum albumin
CCK-8	Cell counting kit-8
CircRNAs	Circular RNAs
cDNA	Complementary DNA
DAB	3,3′-Diaminobenzidine
DAPI	4′,6-Diamidino-2-phenylindole
DMEM	Dulbecco's Modified Eagle Medium
ECL	Enhanced chemiluminescence
EDTA	Ethylenediaminetetraacetic acid
FBS	Fetal bovine serum
FISH	Fluorescence in situ hybridization
FITC	Fluorescein isothiocyanate
GAPDH	Glyceraldehyde-3-phosphate dehydrogenase
gDNA	Genomic DNA
HDAC6	Histone deacetylase 6
HE	Hematoxylin and Eosin
HRP	Horseradish peroxidase
IF	Immunofluorescence
IHC	Immunohistochemistry
LC3	Microtubule-associated protein light chain 3
LDH	Lactate dehydrogenase
miRNA	MicroRNA
MPP^+	1-Methyl-4-phenylpyridinium
MPTP	1-Methyl- 4-phenyl-1, 2, 3, 6-tetrahydropyridine
NC	Negative control
OCT	Optimal cutting temperature
p62/SQSTM1	P62-Sequestosome1
PBS	Phosphate-buffered saline
PD	Parkinson's disease
PI	Propidium iodide
qRT-PCR	Quantitative reverse transcription polymerase chain reaction
Ripa	Radioimmunoprecipitation assay
SD	Standard deviation
shRNA	Short hairpin RNA
TH	Tyrosine hydroxylase
TUNEL	Terminal deoxynucleotidyl transferase Dutp nick end labeling
3′-UTR	3′ Untranslated regions

Acknowledgements

We sincerely appreciate the online databases including circPrimer (https://www.bio-inf.cn/), CircInteractome (https://circinteractome.nia.nih.gov/), and miRDB (http://www.mirdb.org/).

Author contributions

KW conceived and designed the experiments. KW, LZ, and ZR contributed significantly to the experiments and arranging data. KW, LZ, and ZR contributed to project administration, data analyses, visualization and validation. KW wrote the initial draft of the manuscript. LZ revised the manuscript. All authors read and approved the final manuscript.

Funding

This work did not receive any funding support.

Availability of data and material

The datasets generated during and/or analyzed during the current study are available from the corresponding author upon reasonable request.

Declarations

Ethics approval

All the experimental procedures involving animals were conducted following ARRIVE guidelines and approved by the Ethics Committee of the General Hospital of Ningxia Medical University (ethics approval number: 2020–624). The study involving human subjects complied with the Declaration of Helsinki and was approved by the ethical committee of our institution (ethics approval number: 2020–624). All participants provided written informed consent.

Consent for publication

Not applicable.

Competing interests

The authors declare that they have no conflicts of interest.

Author details

[1]Department of Pediatric Surgery, The Affiliated Hospital of Qingdao University, No 16 Jiangsu Road, Qingdao 266000, Shandong, China. [2]Department of Pediatric Surgery, General Hospital of Ningxia Medical University, No 804 Shengli Street, Yinchuan 750000, Ningxia Hui Autonomous Region, China. [3]Department of Pediatric Surgery, General Hospital of Ningxia Medical University, No 804 Shengli Street, Yinchuan 750000, Ningxia Hui Autonomous Region, China.

Received: 25 November 2024 Accepted: 12 May 2025
Published online: 21 May 2025

References

1. Aarsland D, et al. Parkinson disease-associated cognitive impairment. Nat Rev Dis Primers. 2021;7(1):47.
2. Dong-Chen X, et al. Signaling pathways in Parkinson's disease: molecular mechanisms and therapeutic interventions. Signal Transduct Target Ther. 2023;8(1):73.
3. Beitz JM. Parkinson's disease: a review. Front Biosci (Schol Ed). 2014;6(1):65–74.
4. Tolosa E, et al. Challenges in the diagnosis of Parkinson's disease. Lancet Neurol. 2021;20(5):385–97.
5. Li J, et al. Role of circRNAs in neurodevelopment and neurodegenerative diseases. J Mol Neurosci. 2021;71(9):1743–51.
6. Huang W, et al. CircRNA-miRNA networks in regulating bone disease. J Cell Physiol. 2022;237(2):1225–44.
7. Peng F, et al. circRNA_010383 acts as a sponge for miR-135a, and its downregulated expression contributes to renal fibrosis in diabetic nephropathy. Diabetes. 2021;70(2):603–15.
8. Yu L, Liu Y. circRNA_0016624 could sponge miR-98 to regulate BMP2 expression in postmenopausal osteoporosis. Biochem Biophys Res Commun. 2019;516(2):546–50.
9. Li R, et al. CircRNA: a rising star in gastric cancer. Cell Mol Life Sci. 2020;77(9):1661–80.
10. Lan Z-Z, et al. CircPRDM5 inhibits the proliferation, migration, invasion, and glucose metabolism of gastric cancer cells by reducing GCNT4 expression in a miR-485-3p-dependent manner. Kaohsiung J Med Sci. 2024;40(3):231–43.

11. Lu Q, et al. Circ_PRDM5/miR-25-3p/ANKRD46 axis is associated with cell malignant behaviors in subjects with breast cancer evaluated by ultrasound. J Biochem Mol Toxicol. 2023;37(11):e23469.
12. Huang P, Hu Y, Duan Y. TGF-β2-induced circ-PRDM5 regulates migration, invasion, and EMT through the miR-92b-3p/COL1A2 pathway in human lens epithelial cells. J Mol Histol. 2022;53(2):309–20.
13. Liu R, et al. Serum circPRDM5 as a novel diagnostic biomarker for acute myocardial infarction. Gene. 2024;899:148142.
14. Xiao Y, et al. The potential circular RNAs biomarker panel and regulatory networks of Parkinson's Disease. Front Neurosci. 2022;16:893713.
15. Ma B, et al. Mechanisms of circRNA/lncRNA-miRNA interactions and applications in disease and drug research. Biomed Pharmacother. 2023;162:114672.
16. Zhu J, et al. Circular RNA-mediated miRNA sponge & RNA binding protein in biological modulation of breast cancer. Non-coding RNA Res. 2024;9(1):262–76.
17. Burgos K, et al. Profiles of extracellular miRNA in cerebrospinal fluid and serum from patients with Alzheimer's and Parkinson's diseases correlate with disease status and features of pathology. PLoS ONE. 2014;9(5):e94839.
18. Zhang X, et al. Reduced circulating levels of miR-433 and miR-133b are potential biomarkers for Parkinson's Disease. Front Cell Neurosci. 2017;11:170.
19. Zhang L, et al. MicroRNA-433 inhibits the proliferation and migration of HUVECs and neurons by targeting hypoxia-inducible factor 1 alpha. J Mol Neurosci. 2017;61:135–43.
20. Wang R, Zhang J. Clinical significance of miR-433 in the diagnosis of Alzheimer's disease and its effect on Aβ-induced neurotoxicity by regulating JAK2. Exp Gerontol. 2020;141:111080.
21. Bahram Sangani N, et al. A novel insight into neurological disorders through HDAC6 protein–protein interactions. Sci Rep. 2024;14(1):14666.
22. Pandey UB, et al. HDAC6 rescues neurodegeneration and provides an essential link between autophagy and the UPS. Nature. 2007;447(7146):859–63.
23. Yan S, et al. Pharmacological inhibition of HDAC6 attenuates NLRP3 inflammatory response and protects dopaminergic neurons in experimental models of Parkinson's Disease. Front Aging Neurosci. 2020;12:78.
24. d'Ydewalle C, Bogaert E, Van Den Bosch L. HDAC6 at the intersection of neuroprotection and neurodegeneration. Traffic. 2012;13(6):771–9.
25. Hoehn MM, Yahr MD. Parkinsonism: onset, progression and mortality. Neurology. 1967;17(5):427–42.
26. Postuma RB, et al. MDS clinical diagnostic criteria for Parkinson's disease. Mov Disord. 2015;30(12):1591–601.
27. Porrini V, et al. NF-κB/c-Rel DNA-binding is reduced in substantia nigra and peripheral blood mononuclear cells of Parkinson's disease patients. Neurobiol Dis. 2023;180:106067.
28. Serrao M, et al. Prediction of responsiveness of gait variables to rehabilitation training in Parkinson's Disease. Front Neurol. 2019;10:826.
29. Jin ZH, et al. Intermittent theta-burst stimulation combined with physical therapy as an optimal rehabilitation in Parkinson's disease: study protocol for a randomised, double-blind, controlled trial. Trials. 2023;24(1):410.
30. Zhang HY, et al. Transcranial alternating current stimulation improves quality of life in Parkinson's disease: study protocol for a randomized, double-blind, controlled trial. Trials. 2024;25(1):200.
31. Pahwa R, et al. ADS-5102 (amantadine) extended-release capsules for levodopa-induced dyskinesia in Parkinson Disease (EASE LID Study): a randomized clinical trial. JAMA Neurol. 2017;74(8):941–9.
32. Zhao M, et al. The DJ1-Nrf2-STING axis mediates the neuroprotective effects of Withaferin A in Parkinson's disease. Cell Death Differ. 2021;28(8):2517–35.
33. Nadri MH, et al. Antioxidant activities and tyrosinase inhibition effects of *Phaleria macrocarpa* extracts. Afr J Tradit Complement Altern Med. 2014;11(3):107–11.
34. Xiao J, et al. Bioinformatics analysis combined with experimental validation to explore the mechanism of XianLing GuBao capsule against osteoarthritis. J Ethnopharmacol. 2022;294:115292.
35. Daubner SC, Le T, Wang S. Tyrosine hydroxylase and regulation of dopamine synthesis. Arch Biochem Biophys. 2011;508(1):1–12.
36. Zhou Y, et al. CircEPS15, as a sponge of MIR24-3p ameliorates neuronal damage in Parkinson disease through boosting PINK1-PRKN-mediated mitophagy. Autophagy. 2023;19(9):2520–37.
37. Liu Q, et al. circ-Pank1 promotes dopaminergic neuron neurodegeneration through modulating miR-7a-5p/α-syn pathway in Parkinson's disease. Cell Death Dis. 2022;13(5):477.
38. Hanan M, et al. A Parkinson's disease CircRNAs Resource reveals a link between circSLC8A1 and oxidative stress. EMBO Mol Med. 2020;12(9):e11942.
39. Cheng Q, et al. CircSV2b participates in oxidative stress regulation through miR-5107-5p-Foxk1-Akt1 axis in Parkinson's disease. Redox Biol. 2022;56:102430.
40. Liu S, et al. Autophagy: regulator of cell death. Cell Death Dis. 2023;14(10):648.
41. Nechushtai L, Frenkel D, Pinkas-Kramarski R. Autophagy in Parkinson's disease. Biomolecules. 2023;13(10):1435.
42. Hou X, et al. Autophagy in Parkinson's disease. J Mol Biol. 2020;432(8):2651–72.
43. Lizama BN, Chu CT. Neuronal autophagy and mitophagy in Parkinson's disease. Mol Aspects Med. 2021;82:100972.
44. Cheng B, et al. N-acetylcysteine in combination with IGF-1 enhances neuroprotection against proteasome dysfunction-induced neurotoxicity in SH-SY5Y Cells. Parkinsons Dis. 2016;2016:6564212.
45. Zhu JH, et al. Localization of phosphorylated ERK/MAP kinases to mitochondria and autophagosomes in Lewy body diseases. Brain Pathol. 2003;13(4):473–81.
46. Dehay B, et al. Pathogenic lysosomal depletion in Parkinson's disease. J Neurosci. 2010;30(37):12535–44.
47. Dong LI, et al. lncRNA NEAT1 prompts autophagy and apoptosis in MPTP-induced Parkinson's disease by impairing miR-374c-5p. Acta Biochim Biophys Sin (Shanghai). 2021;53(7):870–82.
48. Zuo L, et al. 7,8-dihydroxyflavone ameliorates motor deficits via regulating autophagy in MPTP-induced mouse model of Parkinson's disease. Cell Death Discov. 2021;7(1):254.
49. Su LY, et al. Melatonin attenuates MPTP-induced neurotoxicity via preventing CDK5-mediated autophagy and SNCA/α-synuclein aggregation. Autophagy. 2015;11(10):1745–59.
50. Haghnejad L, et al. Variation in the miRNA-433 binding site of FGF20 is a risk factor for Parkinson's disease in Iranian population. J Neurol Sci. 2015;355(1–2):72–4.
51. Roser AE, et al. Circulating miRNAs as diagnostic biomarkers for Parkinson's Disease. Front Neurosci. 2018;12:625.
52. Chen W, et al. CircMED13L_012 promotes lung adenocarcinoma progression by upregulation of MAPK8 mediated by miR-433-3p. Cancer Cell Int. 2021;21(1):111.
53. Zhao J, et al. HDAC6 deficiency has moderate effects on behaviors and Parkinson's disease pathology in mice. Int J Mol Sci. 2023;24(12):9975.
54. Su M, et al. HDAC6 regulates aggresome-autophagy degradation pathway of α-synuclein in response to MPP+-induced stress. J Neurochem. 2011;117(1):112–20.
55. Garcia J, et al. miR-433-3p suppresses bone formation and mRNAs critical for osteoblast function in mice. J Bone Miner Res. 2021;36(9):1808–22.
56. Jo H, Shim K, Jeoung D. Targeting HDAC6 to overcome autophagy-promoted anti-cancer drug resistance. Int J Mol Sci. 2022;23(17):9592.
57. Simon D, et al. A mutation in the 3′-UTR of the HDAC6 gene abolishing the post-transcriptional regulation mediated by hsa-miR-433 is linked to a new form of dominant X-linked chondrodysplasia. Hum Mol Genet. 2010;19(10):2015–27.
58. Simões-Pires C, et al. HDAC6 as a target for neurodegenerative diseases: what makes it different from the other HDACs? Mol Neurodegener. 2013;8(1):7.
59. English K, Barton MC. HDAC6: a key link between mitochondria and development of peripheral neuropathy. Front Mol Neurosci. 2021;14:684714.

Publisher's Note

Springer Nature remains neutral with regard to jurisdictional claims in published maps and institutional affiliations.